

Modeling of circular integrated optical microresonators by 2-D frequency domain coupled mode theory

K. R. Hiremath, R. Stoffer, M. Hammer

MESA⁺ Institute for Nanotechnology, University of Twente, Enschede, The Netherlands

July 19, 2005

Abstract

Circular integrated optical (ring or disk) microresonators are increasingly employed as compact and versatile wavelength filters. In this paper, we investigate a two dimensional frequency domain model for these devices, based on spatial coupled mode theory. The microresonators are functionally represented in terms of two couplers with appropriate connections using bent and straight waveguides. The abstract scattering matrices of the couplers and the propagation constants of the cavity bends allow to compute the spectral responses of the resonators. Capitalizing on the availability of rigorous analytical modal solutions for bent waveguides, the constituent bent-straight waveguide couplers are modeled using a spatial coupled mode formalism derived by means of a variational principle. The resulting scattering matrices show reciprocity properties as expected according to the symmetry of the coupler structures. We present results for the spectral response and field examples for microresonators with mono- and multi-modal cavities for TE and TM polarizations. Comparisons with finite difference time domain simulations show very good overall agreement.

Keywords: integrated optics, numerical modeling, bent waveguides, bent-straight waveguide couplers, coupled mode theory, circular microresonators

1 Introduction

For already quite some time circular microresonators are discussed as promising building blocks for passive and active components for integrated optical devices [1]. Recent advances in fabrication technology enabled the realization of compact, high finesse resonators, which — in combination with active, nonlinear, electro- or thermo-optic materials — open a range of applications of single or cascaded microring/microdisk resonators e.g. as optical amplifiers or lasers, logic gates, or sensors. Especially, due to their superior selectivity, compactness, and possibility of dense integration, microresonators are considered as attractive add-drop filter elements for applications in photonic chips related to optical wavelength-division multiplexing. Cf. Ref. [2] for a recent overview of the field.

Comprising a ring- or disk-shaped cavity that is evanescently coupled to one or two (parallel or crossed) bus waveguides, circular microresonators are most frequently discussed on the basis of a frequency domain ringresonator model [3, 4], where the interaction between the cavity and the straight waveguides is represented in terms of scattering matrices for the coupler regions. Interferometric resonances are established by segments of bent waveguides that connect these couplers.

On the one hand, this model can be evaluated regarding the coefficients of the coupler scattering matrices and/or the bend mode propagation constants associated with the cavity segments as free parameters. Examples are found in Refs. [5, 3, 6, 7], or in Ref. [8], where a detailed procedure is outlined how to fit the free parameters in the ringresonator model to experimental measurements. Under simplifying assumptions of a lossless coupler and unidirectional monomode wave propagation, universal relations for the coupling of optical power between a cavity ring and one bus waveguide are derived in [9].

On the other hand, one might try to fill the parametric model from first principles, i.e. relate the coupler scattering matrices and the bend mode propagation constants to the device geometry and material properties, as it is

essential for a quantitative resonator design. Rather few studies exist; among these are e.g. Refs. [10, 11], which differ with respect to the methods and approximations that are employed to obtain the modal basis solutions for the curved cavity segments, and to predict the interaction between the cavity and the bus waveguides. For the latter task, approaches based on coupled mode theory (CMT) [12, 13] are applied.

In the present paper we investigate an ab initio two-dimensional frequency domain spatial CMT model that is as far as possible a straightforward implementation of the conventional ringresonator viewpoint. The simulations rely on analytically computed modal solutions for bent waveguides and curved interfaces [14], separable fields for given real frequency with complex angular propagation constants. Due to the angular field decay and non-integer azimuthal mode numbers these do not constitute valid solutions for the full rotationally symmetric cavities, i.e. do not allow to access directly the (complex) resonance frequencies of the isolated cavities. Still one can construct approximations to solutions of scattering problems on the basis of these fields, if the interaction with the straight waveguides is taken into account. The bend mode profiles decay suitably fast in the radial direction [14], such that these bend modes can be conveniently used as basis fields in a frequency domain coupled mode description. The coupled mode equations are derived from first principles by variational means. Preliminary results are contained in Refs. [4, 15]; here we also extend the approach to configurations with multimode constituent waveguides.

While for specific configurations one could regard the present two dimensional model as an approximate description of realistic devices in terms of effective indices [11], in other cases simulations in three spatial dimensions are certainly necessary, e.g. for vertically coupled resonators. Therefore our model is formulated such that an extension to three dimensions is straightforward; corresponding results are presented elsewhere [16]. Note that the theoretical arguments for 2-D and 3-D resonators are (almost) identical. For the 3-D simulations, the computation of basis fields, i.e. mode profiles of straight and bent waveguides with 2-D cross sections, is a nontrivial and time consuming task, while for the 2-D setting, sound analytical basis fields are available. Concerning benchmarking rigorous numerical calculations exist for the 2-D setting, which are not available in 3-D. Therefore for the present paper, we chose 2-D resonators for the introduction and assessment of the CMT formulation.

The paper is organized as follows. Section 2 introduces the schematic microresonator model, formulated directly for configurations with multimode cavities. One of the essential ingredients are representations of the interaction regions between bent and straight waveguides. The CMT model for these couplers is described in Section 3. Section 4 outlines how to compute the spectral response of the resonators. Section 5 provides a series of example simulations, including the benchmarking against independent rigorous numerical calculations.

Referring to the classification of resonator types given in [17], we treat the circular microcavities as traveling wave resonators in the framework of a pure frequency domain description. Neglecting reflected waves turns out to be adequate even for the present devices with already quite small radii (though we can check this only implicitly via comparison to numerical results). One expects this approximation to break down for even smaller cavities, where the interaction between the waves in the bus waveguides and the cavity can no longer be regarded as adiabatic. In that regime of standing wave resonators descriptions similar to those given in Refs. [17, 18] would have to be applied, that take reflected waves fully into account.

The present approach differs from the viewpoint of time domain models [19, 17] based on (time-domain) modes for the entire circular cavities. These are solutions with integer rotational mode number and complex frequency [10, 20, 21]. Problems for a coupled mode description arise from the radially growing field solutions of the time-domain modes [20, 21], although it is partially possible to translate between the two viewpoints [10, 20].

Alternatively numerical tools like Finite Difference Time Domain (FDTD) methods [22, 23] can be employed; we apply a FDTD implementation [24, 25] for benchmarking purposes. In [25] a finite-difference Helmholtz solver is used to compute the spectral response of two dimensional microdisk-resonators. However, already in the two dimensional setting these pure numerical methods turn out to be inconveniently time consuming; the computational effort required in three dimensions must be expected to be prohibitive for practical design work.

Finally one should emphasize that specific 2-D configurations can be treated in an accurate and highly efficient analytical way in terms of integral equations [26]. This concerns eigenvalue [27, 28] and scattering problems [29, 30] for micro-ring and disk cavities with regular deformations, in the vicinity of one straight dielectric

waveguide or half-block. Unfortunately, the extension to three dimensions appears to be far from obvious.

Apart from the circular structures, resonators with other shapes of cavities are also investigated [31, 32, 18, 33]. In case of traveling wave resonators [17], if suitable basis fields for the CMT analysis are conveniently computable, then in principle the CMT approach described in this paper can be adapted to these shapes. This applies in particular to resonators with racetrack shaped cavities [33], in which each coupler section consists of a parallel straight waveguide coupler, in between two “half” bent-straight waveguide couplers. The CMT approach of Section 3 should be applicable to these individual coupler segments, where the transitions between straight and curved pieces [34] of the cavity should be treated adequately, e.g. in terms of suitable projections.

2 Abstract microresonator model

The resonator elements investigated in this paper consist of ring- or disk shaped dielectric cavities, evanescently coupled to two parallel straight bus cores. We consider guided-wave scattering problems in the frequency domain, where a time-harmonic optical signal $\sim \exp(i\omega t)$ of given real frequency ω is present everywhere. Cartesian coordinates x, z are introduced for the spatially two dimensional description as shown in Figure 1. The structure and all TE- or TM-polarized optical fields are assumed to be constant in the y -direction.

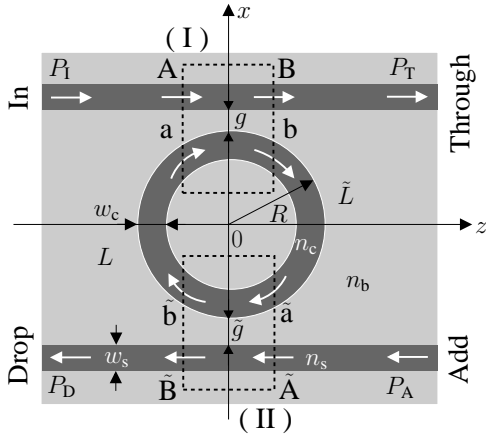


Figure 1: Schematic microresonator representation: A cavity of radius R , core refractive index n_c and width w_c is placed between two straight waveguides with core refractive index n_s and width w_s , with gaps of width g and \tilde{g} between the cavity and the bus waveguides. n_b is the background refractive index. The device is divided into two couplers (I), (II), connected by cavity segments of lengths L and \tilde{L} outside the coupler regions.

Adhering to the most common description for microring-resonators [3, 4], the devices are divided into two bent-straight waveguide couplers, which are connected by segments of the cavity ring. Half-infinite pieces of straight waveguides constitute the external connections, where the letters $A, B, \tilde{A}, \tilde{B}$ (external) and $a, b, \tilde{a}, \tilde{b}$ (internal) denote the coupler ports. If one accepts the approximation that the interaction between the optical waves in the cavity and in the bus waveguides is negligible outside the coupler regions, then this functional decomposition reduces the microresonator description to the mode analysis of straight and bent waveguides, and the modeling of the bent-straight waveguide couplers.

Assuming that all transitions inside the coupler regions are sufficiently smooth, such that reflections do not play a significant role for the resonator functioning, we further restrict the model to unidirectional wave propagation, as indicated by the arrows in Figure 1. Depending on the specific configuration, this assumption can be justified or not; at least for the structures considered in Section 5 we observed this approximation to be adequate.

Consider coupler (I) first. Suppose that the straight cores support N_s guided modes with propagation constants β_{sq} , $q = 1, \dots, N_s$. For the cavity, N_b bend modes are taken into account. Due to the radiation losses, their propagation constants $\gamma_{bp} = \beta_{bp} - i\alpha_{bp}$, $p = 1, \dots, N_b$, are complex valued [14]. Here β_{sq} , β_{bp} and α_{bp} are real positive numbers. The variables A_q, B_q , and a_p, b_p , denote the directional amplitudes of the properly normalized “forward” propagating (clockwise direction, cf. Figure 1) basis modes in the respective coupler port planes, combined into amplitude (column) vectors \mathbf{A}, \mathbf{B} , and \mathbf{a}, \mathbf{b} .

Now the abstract functioning of coupler (I) can be represented in terms of a scattering matrix, that relates the (bidirectional) amplitudes of the outgoing waves to the amplitudes of the corresponding given incoming modes:

$$\begin{pmatrix} a^- \\ A^- \\ b \\ B \end{pmatrix} = \begin{pmatrix} 0 & 0 & S_{bb}^- & S_{bs}^- \\ 0 & 0 & S_{sb}^- & S_{ss}^- \\ S_{bb} & S_{bs} & 0 & 0 \\ S_{sb} & S_{ss} & 0 & 0 \end{pmatrix} \begin{pmatrix} a \\ A \\ b^- \\ B^- \end{pmatrix}. \quad (1)$$

Here the superscripts $-$ indicate the amplitudes of backwards (anticlockwise) propagating waves, where the zeroes implement the assumption of negligible backreflections. The entries of the submatrices S_{vw} with $v, w = b, s$ represent the “coupling” from the modes of waveguide w to the fields supported by waveguide v .

A fundamental property of any linear optical circuit made of nonmagnetic materials is that the transmission between any two “ports” does not depend upon the propagation direction. The proof can be based e.g. on the integration of a reciprocity identity over the spatial domain covered by that circuit [12]. More specifically, the full scattering matrix of the reciprocal circuit has to be symmetric. The argument holds for circuits with potentially attenuating materials, in the presence of radiative losses, and irrespectively of the particular shape of the connecting cores. It relies crucially on the precise definition of the “ports” of the circuit, where independent ports can be realized either by mode orthogonality or by spatially well separated outlets.

Assuming that the requirements of that argument can be applied at least approximately to our present bent-straight waveguide couplers, one expects that the coupler scattering matrix is symmetric. For the submatrices this implies the following equalities (T denotes the transpose):

$$S_{bb} = (S_{bb}^-)^T, \quad S_{sb} = (S_{bs}^-)^T, \quad S_{bs} = (S_{sb}^-)^T, \quad S_{ss} = (S_{ss}^-)^T. \quad (2)$$

If coupler (I) is defined symmetrical with respect to the central plane $z = 0$ and if identical mode profiles are used for the incoming and outgoing fields, then one can further expect (see [12]) the transmission $A \rightarrow b$ to be equal to the transmission $B^- \rightarrow a^-$. Similarly, one expects equal transmissions $a \rightarrow B$ and $b^- \rightarrow A^-$, or

$$S_{bs} = S_{bs}^-, \quad S_{sb} = S_{sb}^-. \quad (3)$$

Consequently, according to equations (2) and (3), also the unidirectional scattering matrix

$$S = \begin{pmatrix} S_{bb} & S_{bs} \\ S_{sb} & S_{ss} \end{pmatrix} \quad (4)$$

associated with the forward, clockwise propagation through coupler (I), i.e. the lower left quarter block of the full matrix in equation (1) can be expected to be symmetric:

$$S_{bs} = (S_{sb})^T, \quad S_{bs}^- = (S_{sb}^-)^T. \quad (5)$$

“The coupling from the straight waveguide to the cavity is equal to the coupling from the cavity bend to the bus waveguide”, here translated to the multimode setting.

A completely analogous reasoning applies to the second coupler, where a symbol $\tilde{\cdot}$ identifies the mode amplitudes \tilde{A} , \tilde{B} , and \tilde{a} , \tilde{b} , at the port planes and the unidirectional scattering matrix \tilde{S} related to coupler (II), such that the coupler operation is represented as

$$\begin{pmatrix} b \\ B \end{pmatrix} = S \begin{pmatrix} a \\ A \end{pmatrix}, \quad \begin{pmatrix} \tilde{b} \\ \tilde{B} \end{pmatrix} = \tilde{S} \begin{pmatrix} \tilde{a} \\ \tilde{A} \end{pmatrix}. \quad (6)$$

Outside the coupler regions the bend modes used for the description of the field in the cavity propagate independently, with the angular / arc-length dependence given by their propagation constants (cf. equation (10)). Hence the amplitudes at the entry and exit ports of the connecting cavity segments are related to each other as

$$a = G \tilde{b} \quad \text{and} \quad \tilde{a} = \tilde{G} b, \quad (7)$$

where G and \tilde{G} are $N_b \times N_b$ diagonal matrices with entries $G_{p,p} = \exp(-i\gamma_{bp}L)$ and $\tilde{G}_{p,p} = \exp(-i\gamma_{bp}\tilde{L})$, respectively, for $p = 1, \dots, N_b$.

For the guided wave scattering problem, modal powers $P_{Iq} = |A_q|^2$ and $P_{Aq} = |\tilde{A}_q|^2$ are prescribed at the In-port A and at the Add-port \tilde{A} of the resonator, and one is interested in the transmitted powers $P_{Tq} = |B_q|^2$ at port B and the backward dropped powers $P_{Dq} = |\tilde{B}_q|^2$ at port \tilde{B} . The linear system established by equations (6) and (7) is to be solved for \mathbf{B} and $\tilde{\mathbf{B}}$, given values of \mathbf{A} and $\tilde{\mathbf{A}}$. Due the linearity of the device the restriction to an excitation in only one port, here port A, with no incoming Add-signal $\tilde{\mathbf{A}} = \mathbf{0}$, is sufficient. One obtains

$$\mathbf{B} = (\mathbf{S}_{sb} \mathbf{G} \tilde{\mathbf{S}}_{bb} \tilde{\mathbf{G}} \Omega^{-1} \mathbf{S}_{bs} + \mathbf{S}_{ss}) \mathbf{A}, \quad \tilde{\mathbf{B}} = (\tilde{\mathbf{S}}_{sb} \tilde{\mathbf{G}} \Omega^{-1} \mathbf{S}_{bs}) \mathbf{A} \quad (8)$$

for the amplitudes of the outgoing guided modes in the Through- and Drop-ports, and

$$\mathbf{b} = \Omega^{-1} \mathbf{S}_{bs} \mathbf{A}, \quad \tilde{\mathbf{b}} = \tilde{\mathbf{S}}_{bb} \tilde{\mathbf{G}} \Omega^{-1} \mathbf{S}_{bs} \mathbf{A} \quad (9)$$

for the internal mode amplitudes in the cavity, where $\Omega = \mathbf{I} - \mathbf{S}_{bb} \mathbf{G} \tilde{\mathbf{S}}_{bb} \tilde{\mathbf{G}}$.

Among the factors in the expressions (8) and (9) only the inverse of Ω can be expected to introduce a pronounced wavelength dependence. Thus Ω^{-1} can be viewed as a resonance denominator in matrix form; resonances appear in case Ω becomes nearly singular, i.e. exhibits an eigenvalue close to zero. This “resonance condition” permits a quite intuitive interpretation: Resonances appear if a field amplitude vector is excited inside the cavity, that corresponds to a close-to-zero eigenvalue of Ω , or a unit eigenvalue of $\mathbf{S}_{bb} \mathbf{G} \tilde{\mathbf{S}}_{bb} \tilde{\mathbf{G}}$. That relates to a field which reproduces itself after propagating consecutively along the right cavity segment, through coupler (II), along the left cavity segment, and finally through coupler (I).

In general resonances must be expected to involve all bend modes that are taken into account for the description of the cavity field, due to the interaction caused by the presence of the straight cores (cf. e.g. the example of the hybrid cavity ring given in Ref. [16]). If, however, this direct interaction between the bend modes is weak, the matrices \mathbf{S}_{bb} and $\tilde{\mathbf{S}}_{bb}$ become nearly diagonal just like \mathbf{G} and $\tilde{\mathbf{G}}$, and resonances can be ascribed to individual cavity modes. Analogously to the case of standing wave resonators [18], this viewpoint allows a quantitative characterization of resonances associated with “almost isolated” cavities, where the bus waveguides are absent. Also for the numerical examples in Section 5.5 we found this regime to be realized; resonances can be classified as belonging to specific bend modes by inspecting the mode amplitudes that establish inside the cavity at the resonance wavelength.

In case of a configuration with single mode cavity and bus cores, further evaluation of expressions (8) and (9) is fairly standard [3, 4]; one obtains the familiar explicit, parameterized expressions for the transmitted and dropped power, for the free spectral range and the resonance width, for finesse and Q-factor of the resonances, etc. Here the above resonance condition means that at coupler (I) the incoming signal from the bus waveguide is in phase with the wave propagating already along the cavity, and that it compensates the propagation loss of the cavity round trip. Resonances appear as a drop in the directly transmitted power P_T , and a simultaneous peak in the dropped power P_D . Assuming that this reasoning is also applicable to a multimode configuration with weak interaction, one can establish separate resonance conditions for the individual cavity modes, which in general will be satisfied at different wavelengths. The power spectrum of the microresonator shows a systematically repeating pattern with multiple extrema, where each resonance corresponds to cavity modes of different orders. See Figure 13 for an example.

According to equations (8) and (9), a quantitative evaluation of the present microresonator model requires the propagation constants of the cavity modes γ_{bp} , hidden in \mathbf{G} , $\tilde{\mathbf{G}}$, and the scattering matrices \mathbf{S} , $\tilde{\mathbf{S}}$ of couplers (I) and (II). Computation of the latter is the subject of the following section.

3 Bent-straight waveguide couplers

One of the many variants of coupled mode theory [12, 13] will be applied here as a simple and intuitive tool for the modeling of the interaction of optical waves in the bent-straight waveguide couplers. The formulation takes into account that multiple modes in each of the cores may turn out to be relevant for the functioning of the resonators. A preliminary version for single-mode waveguides has been described in Refs. [4, 15].

Consider the coupler configuration shown in Figure 2(a). The CMT description starts with the specification of the basis fields, here the time-harmonic modal solutions associated with the isolated bent (b) and straight cores

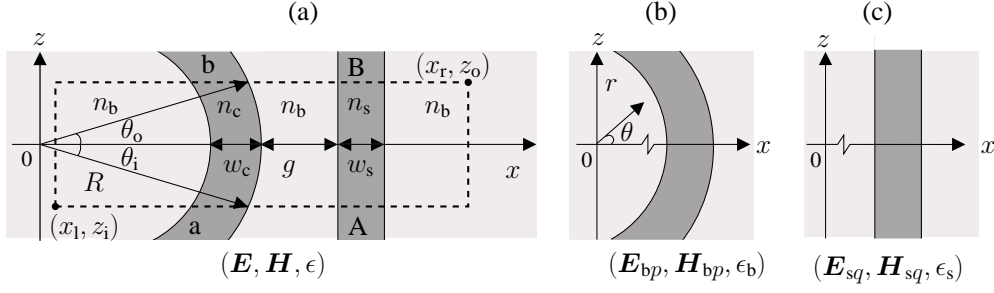


Figure 2: The bent-straight waveguide coupler setting (a), coupler (I) of Figure 1. One assumes that the interaction between the waves supported by the bent and straight cores is restricted to the rectangular computational window $[x_l, x_r] \times [z_i, z_o]$. Inside this region the optical field is represented as a linear combination of the modal fields of the bent waveguide (b) and of the straight waveguide (c).

(c). Customarily, the real, positive frequency ω is given by the vacuum wavelength λ ; we omit the common time dependence $\sim \exp(i\omega t)$ for the sake of brevity. In line with the assumptions of Section 2 only forward propagating modes are considered, where, for convenience, we choose the z -axis of the Cartesian system as introduced in Figure 2 as the common propagation coordinate for all fields.

Let \mathbf{E}_{bp} , \mathbf{H}_{bp} , and ϵ_b represent the modal electric fields, magnetic fields, and the spatial distribution of the relative permittivity of the bent waveguide. Due to the rotational symmetry these fields are naturally given in the polar coordinate system r, θ associated with the bent waveguide. For the application in the CMT formalism, the polar coordinates are expressed in the Cartesian x - z -system, such that the basis fields for the cavity read

$$\begin{pmatrix} \mathbf{E}_{bp} \\ \mathbf{H}_{bp} \end{pmatrix}(x, z) = \begin{pmatrix} \tilde{\mathbf{E}}_{bp} \\ \tilde{\mathbf{H}}_{bp} \end{pmatrix}(r(x, z)) e^{-i\gamma_{bp} R \theta(x, z)}. \quad (10)$$

Here $\tilde{\mathbf{E}}_{bp}$ and $\tilde{\mathbf{H}}_{bp}$ are the radial dependent electric and magnetic parts of the mode profiles; the complex propagation constants γ_{bp} prescribe the harmonic dependences on the angular coordinate. Note that the actual values of γ_{bp} are related to the (arbitrary) definition of the bend radius R [14].

Likewise, \mathbf{E}_{sq} , \mathbf{H}_{sq} , and ϵ_s denote the modal fields and the relative permittivity associated with the straight waveguide. These are of the form

$$\begin{pmatrix} \mathbf{E}_{sq} \\ \mathbf{H}_{sq} \end{pmatrix}(x, z) = \begin{pmatrix} \tilde{\mathbf{E}}_{sq} \\ \tilde{\mathbf{H}}_{sq} \end{pmatrix}(x) e^{-i\beta_{sq} z}, \quad (11)$$

i.e. guided modes with profiles $\tilde{\mathbf{E}}_{sq}$, $\tilde{\mathbf{H}}_{sq}$ that depend on the lateral coordinate x , multiplied by the appropriate harmonic dependence on the longitudinal coordinate z , with positive propagation constants β_{sq} . Note that for the present 2-D theory all modal solutions can be computed analytically. While the modal analysis is fairly standard for straight multilayer waveguides with piecewise constant permittivity, for the bend structures we employ analytic solutions in terms of Bessel- and Hankel functions of complex order, computed by means of a bend mode solver as presented in Ref. [14].

Now the total optical electromagnetic field \mathbf{E} , \mathbf{H} inside the coupler region is assumed to be well represented by a linear combination of the modal basis fields (10), (11),

$$\begin{pmatrix} \mathbf{E} \\ \mathbf{H} \end{pmatrix}(x, z) = \sum_{v=b,s} \sum_{i=1}^{N_v} C_{vi}(z) \begin{pmatrix} \mathbf{E}_{vi} \\ \mathbf{H}_{vi} \end{pmatrix}(x, z) \quad (12)$$

with so far unknown amplitudes C_{vi} that are allowed to vary with the propagation coordinate z . This assumption forms the central approximation of the present CMT approach; no further approximations or heuristics enter, apart from the numerical procedures used for the evaluation of the CMT equations (section 5.1). Note that here, unlike e.g. in Ref. [10], no “phase matching” arguments appear; via the transformation $r, \theta \rightarrow x, z$ the tilt of the wave front of the bend modes (10) is taken explicitly into account.

For the further procedures, the unknown functions C_{vi} are combined into amplitude vectors $\mathbf{C} = (\mathbf{C}_b, \mathbf{C}_s) = ((C_{bi}), (C_{si}))$. To determine equations for these unknowns, here we follow an approach that relies on a variational principle. Consider the functional

$$\mathcal{F}(\mathbf{E}, \mathbf{H}) = \iint [(\nabla \times \mathbf{E}) \cdot \mathbf{H}^* - (\nabla \times \mathbf{H}) \cdot \mathbf{E}^* + i\omega\mu_0 \mathbf{H} \cdot \mathbf{H}^* + i\omega\epsilon_0 \mathbf{E} \cdot \mathbf{E}^*] dx dz, \quad (13)$$

a 2-D restriction of the functional for the 3-D setting given in [12], stripped from the boundary terms. For the present 2-D configurations, the convention of vanishing derivatives $\partial_y = 0$ applies to all fields; the curl-operators are to be interpreted accordingly. \mathcal{F} is meant to be viewed as being dependent on the six field components \mathbf{E}, \mathbf{H} . If \mathcal{F} becomes stationary with respect to arbitrary variations of these arguments, then \mathbf{E} and \mathbf{H} satisfy the Maxwell curl equations as a necessary condition:

$$\nabla \times \mathbf{E} = -i\omega\mu_0 \mathbf{H}, \quad \nabla \times \mathbf{H} = i\omega\epsilon_0 \mathbf{E}. \quad (14)$$

We now restrict the functional to the fields allowed by the coupled mode ansatz. After inserting the trial field (12) into the functional (13), \mathcal{F} becomes a functional that depends on the unknown amplitudes \mathbf{C} . For the “best” approximation to a solution of the problem (14) in the form of the field (12), the variation of $\mathcal{F}(\mathbf{C})$ is required to vanish for arbitrary variations $\delta\mathbf{C}$. Disregarding again some boundary terms, the first variations of \mathcal{F} at \mathbf{C} in the directions δC_{wj} , for $j = 1, \dots, N_w$ and $w = b, s$, are

$$\delta\mathcal{F} = \int \sum_{v=b,s} \sum_{i=1}^{N_v} \{M_{vi,wj} dz C_{vi} - F_{vi,wj} C_{vi}\} \delta C_{wj}^* dz - c.c. \quad (15)$$

where *c.c.* indicates the complex conjugate of the preceding integrated term,

$$M_{vi,wj} = \langle \mathbf{E}_{vi}, \mathbf{H}_{vi}; \mathbf{E}_{wj}, \mathbf{H}_{wj} \rangle = \int \mathbf{a}_z \cdot (\mathbf{E}_{vi} \times \mathbf{H}_{wj}^* + \mathbf{E}_{wj}^* \times \mathbf{H}_{vi}) dx, \quad (16)$$

$$F_{vi,wj} = -i\omega\epsilon_0 \int (\epsilon - \epsilon_v) \mathbf{E}_{vi} \cdot \mathbf{E}_{wj}^* dx, \quad (17)$$

and where \mathbf{a}_z is a unit vector in the z -direction. Consequently, one arrives at the coupled mode equations

$$\sum_{v=b,s} \sum_{i=1}^{N_v} M_{vi,wj} dz C_{vi} - \sum_{v=b,s} \sum_{i=1}^{N_v} F_{vi,wj} C_{vi} = 0, \quad \text{for } j = 1, \dots, N_w, \text{ and } w = b, s, \quad (18)$$

as a necessary condition for \mathcal{F} to become stationary for arbitrary variations δC_{wj} . Note that the same expression is also obtained from the complex conjugate part of equation (15). In matrix notation, equations (18) read

$$\mathbf{M}(z) dz \mathbf{C}(z) = \mathbf{F}(z) \mathbf{C}(z). \quad (19)$$

Here the entries of the matrices \mathbf{M} and \mathbf{F} are given by the integrals (16) and (17). Due to the functional form of the bend modes and the varying distance between the bent and straight cores, these coefficients are z -dependent. Coupled mode equations identical to (18) or (19), respectively, can be derived by means of a reciprocity identity [12], as detailed in Ref. [35]. See Refs. [15, 4] for explicit representations of these equations in the single mode case $N_b = N_s = 1$.

To proceed further, the CMT equations are solved by numerical means. Brief details about the procedures are given in Section 5.1; the result can be stated in terms of a transfer matrix \mathbf{T} that relates the CMT amplitudes at the output plane $z = z_o$ to the amplitudes at the input plane $z = z_i$ of the coupler region:

$$\mathbf{C}(z_o) = \mathbf{T} \mathbf{C}(z_i). \quad (20)$$

It remains to relate the transfer matrix, obtained directly as the solution of the CMT equations on the limited computational window, to the coupler scattering matrix as required for the abstract model of Section 2.

Outside the coupler (i.e. outside the region $[x_1, x_r] \times [z_i, z_o]$), it is assumed that the interaction between the fields associated with the different cores is negligible. The individual modes propagate undisturbed according to the harmonic dependences on the respective propagation coordinates, such that the external fields are:

$$\begin{aligned} a_p \begin{pmatrix} \tilde{\mathbf{E}}_{bp} \\ \tilde{\mathbf{H}}_{bp} \end{pmatrix}(r) e^{-i\gamma_{bp}R(\theta - \theta_i)}, \text{ for } \theta \leq \theta_i, & \quad A_q \begin{pmatrix} \tilde{\mathbf{E}}_{sq} \\ \tilde{\mathbf{H}}_{sq} \end{pmatrix}(x) e^{-i\beta_{sq}(z - z_i)}, \text{ for } z \leq z_i, \\ b_p \begin{pmatrix} \tilde{\mathbf{E}}_{bp} \\ \tilde{\mathbf{H}}_{bp} \end{pmatrix}(r) e^{-i\gamma_{bp}R(\theta - \theta_o)}, \text{ for } \theta \geq \theta_o, & \quad B_q \begin{pmatrix} \tilde{\mathbf{E}}_{sq} \\ \tilde{\mathbf{H}}_{sq} \end{pmatrix}(x) e^{-i\beta_{sq}(z - z_o)}, \text{ for } z \geq z_o. \end{aligned} \quad (21)$$

Here \mathbf{a} , \mathbf{A} and \mathbf{b} , \mathbf{B} are the constant external mode amplitudes at the input and output ports of the coupler, as introduced in Section 2. See Figure 2 for the definitions of the coordinate offsets z_i , θ_i and z_o , θ_o .

For a typical coupler configuration, the guided modal fields of the straight waveguide are well confined to the straight core. On the contrary, due to the radiative nature of the fields, the bend mode profiles can extend far beyond the outer interface of the bent waveguide. Depending upon the specific physical configuration, the extent of these radiative parts of the fields varies, such that also outside the actual coupler region the field strength of the bend modes in the region close to the straight core may be significant. Therefore, to assign the external mode amplitudes A_q , B_q , it turns out to be necessary to project the coupled field on the straight waveguide modes.

At a sufficient distance from the cavity, in the region where only the straight waveguide is present, the total field $\phi = (\mathbf{E}, \mathbf{H})$ can be expanded into the complete set of modal solutions of the eigenvalue problem for the straight waveguide. The basis set consists of a finite number of guided modes $\phi_{sq} = (\mathbf{E}_{sq}, \mathbf{H}_{sq})$ and a nonguided, radiative part ϕ_{rad} , such that $\phi = \sum_q B_q \phi_{sq} + \phi_{rad}$, where B_q are the constant amplitudes of ϕ_{sq} . These amplitudes can be extracted by applying the formal expansion to the total field (12) as given by the solution of the CMT equations. Using the orthogonality properties of the basis elements, the projection at the output plane $z = z_o$ of the coupler yields

$$B_q \exp(i\beta_{sq}z) = C_{sq} + \sum_{p=1}^{N_b} C_{bp} \frac{\langle \phi_{bp}; \phi_{sq} \rangle}{\langle \phi_{sq}; \phi_{sq} \rangle} = C_{sq} + \sum_{p=1}^{N_b} C_{bp} \frac{M_{bp,sq}}{M_{sq,sq}}. \quad (22)$$

where the mode overlaps $\langle \phi_{mi}; \phi_{nj} \rangle = \langle \mathbf{E}_{mi}, \mathbf{H}_{mi}; \mathbf{E}_{nj}, \mathbf{H}_{nj} \rangle = M_{mi,nj}$ occur already in the coupled mode equations (19). An expression analogous to (22) can be written for the projection at $z = z_i$, where the coefficients A_q are involved. What concerns the external amplitudes of the bend modes, no such procedure is required, since the field strengths of the straight waveguide modes is usually negligible in the respective angular planes, where the major part of the bend mode profiles is located. Here merely factors are introduced that adjust the offsets of the angular coordinates in (21).

Thus, given the solution (20) of the coupled mode equations in the form of the transfer matrix \mathbf{T} , the scattering matrix \mathbf{S} that relates the amplitudes a_p , b_p , A_q , B_q of the external fields as required in equation (6) is defined as

$$\mathbf{S} = \mathbf{Q} \mathbf{T} \mathbf{P}^{-1} \quad (23)$$

where \mathbf{P} and \mathbf{Q} are $(N_b + N_s) \times (N_b + N_s)$ matrices with diagonal entries $P_{p,p} = \exp(-i\gamma_{bp}R\theta_i)$ and $Q_{p,p} = \exp(-i\gamma_{bp}R\theta_o)$, for $p = 1, \dots, N_b$, followed by $P_{q+N_b,q+N_b} = \exp(-i\beta_{sq}z_i)$ and $Q_{q+N_b,q+N_b} = \exp(-i\beta_{sq}z_o)$, for $q = 1, \dots, N_s$. A lower left block is filled with elements $P_{q+N_b,p} = \exp(-i\beta_{sq}z)$ $M_{bp,sq}/M_{sq,sq}|_{z=z_i}$ and $Q_{q+N_b,p} = \exp(-i\beta_{sq}z)$ $M_{bp,sq}/M_{sq,sq}|_{z=z_o}$, for $q = 1, \dots, N_s$ and $p = 1, \dots, N_b$, respectively, that incorporate the projections. All other coefficients of \mathbf{P} and \mathbf{Q} are zero.

Admittedly, at the first glance the projection operation might appear redundant, since the CMT solution in the form (12) provides directly amplitudes for the basis fields that occur also in the external field representation (21). Here perhaps further explanatory remarks are necessary.

The physical field around the exit planes of the CMT window can be seen as a superposition of the outgoing guided modes of the bus core with their constant amplitudes, and a remainder, that, when expanded in the modal

basis associated with the straight waveguide, is orthogonal to the guided waves. The notions of “vanishing interaction” or “decoupled” fields, as used e.g. for the motivation of the assumptions underlying the abstract framework of Section 2, are to be concretized in precisely this way: The guided waves in the straight core are stationary, iff projections onto the mode profiles at growing propagation distances lead to constant amplitudes A_q, B_q (apart from the phase changes according to the undisturbed propagation of the respective modes).

Now the CMT formalism is limited to the few non-orthogonal bend and straight modes included in the CMT ansatz, which are overlapping in the regions of the input and exit ports A and B of the coupler. Consequently, when the CMT procedures try to approximate both the guided and radiative part of the real field, the optimum approximations may well be superpositions with non-stationary coupled mode amplitudes C_{sq} of the modes of the bus waveguide. Indeed, as observed in Sections 5.2 and 5.4, the projected amplitudes $|B_q|^2$ (or the related scattering matrix elements $|S_{sq,wj}|^2$) become stationary, when viewed as a function of the exit port position z_o , while at the same time the associated CMT solution $|C_{sq}(z)|^2$ (or the elements $|T_{sq,wj}|^2$ of the transfer matrix) exhibit an oscillatory behaviour. Still, in the sense of the projections, one can speak of “non-interacting, decoupled” fields. That justifies the limitation of the computational window to z -intervals where the elements of \mathbf{S} (not necessarily of \mathbf{T}) attain constant absolute values around the input and output planes.

In conclusion, it is at least partly misleading to stick to the familiar notion of “mode evolutions” computed by the CMT approach. If one abandons that viewpoint and regards the CMT procedures as just “a” method that generates an approximate field solution inside the computational window, then applying the projections to extract the external mode amplitudes appears perfectly reasonable.

4 Spectrum evaluation

Once the propagation constants of the cavity modes and the coupler scattering matrices are available, the optical transmission through the resonator is given by equations (8). In principle the spectral response of the device can be obtained by repeating the entire solution procedure for different wavelengths in an interesting range.

That direct approach requires repeated computations of the bend propagation constants and the scattering matrices. A large part of the numerical effort can be avoided, if one calculates the relevant quantities merely for a few distant wavelengths, and then uses complex interpolations of these values for the actual spectrum evaluation. The interpolation procedure, however, should be applied to quantities that vary but slowly with the wavelength.

In line with the reasoning concerning the resonances at the end of section 2, one can expect that any rapid wavelength dependence of the transmission is determined mainly by the phase gain of the waves circulating in the cavity. Rapid changes in these phase relations are due to a comparably slow wavelength dependence of the bend propagation constants γ_{bp} , that is multiplied by the lengths L, \tilde{L} of the external cavity segments. If a substantial part of the cavity is already contained in the coupler regions, then the elements of the scattering matrices \mathbf{S} exhibit also fast phase oscillations with the wavelength, such that \mathbf{S} directly is not suitable for the interpolation. Apart from these rapid changes, which can be attributed to the unperturbed propagation of the basis modes along the bent and straight waveguides, the interaction between the waves in the two coupled cores introduces an additional wavelength dependence, which in turn can be expected to be slow.

To separate the two scales of wavelength dependence in \mathbf{S} , one divides by the exponentials that correspond to the undisturbed wave propagation of the bend and straight modes towards and from the symmetry plane $z = 0$:

$$\mathbf{S}' = \mathbf{Q}^0 \mathbf{S} (\mathbf{P}^0)^{-1} \quad (24)$$

Here \mathbf{P}^0 and \mathbf{Q}^0 are diagonal matrices with entries $P_{j,j}^0$ and $Q_{j,j}^0$ as defined for \mathbf{P} and \mathbf{Q} in equation (23). Formally, one can view \mathbf{S}' as the scattering matrix of a coupler with zero length, where the interaction takes place instantaneously at $z = 0$. This modification of \mathbf{S} , applied analogously to $\tilde{\mathbf{S}}$, is compensated by redefining the lengths of the external cavity segments as $L' = \tilde{L}' = \pi R$, by changing the matrices \mathbf{G} and $\tilde{\mathbf{G}}$ accordingly, and, where necessary, by taking into account the altered phase relations on the external straight segments.

After these modifications, the new matrices \mathbf{G}' and $\tilde{\mathbf{G}}'$ capture the phase gain of the cavity field along the full

circumference. The modified scattering matrices \mathbf{S}' and $\tilde{\mathbf{S}}'$ show only a slow wavelength dependence, such that the interpolation can be successfully applied to these matrices and to the bend propagation constants in \mathbf{G}' and $\tilde{\mathbf{G}}'$. The resonant features of the device are now entirely effected by the analytical relations (8), such that one obtains an excellent agreement between the transmission spectra computed with the interpolated quantities and the direct calculation, while the computational effort is significantly reduced.

5 Simulation results

Having explained how to compute the scattering matrices for the bent-straight waveguide couplers and how to use them along with analytic modal solutions for the straight bus waveguides and the cavity bends [14] to assemble the spectral response the resonator devices, in this section we summarize a series of numerical results for the theory outlined in Sections 2, 3, and 4.

Note that the test cases have been chosen such that reliable benchmark solutions can be computed with reasonable effort by means of standard FDTD calculations. Quite compact disk- or ring-cavities with substantial refractive index contrast are considered. For the CMT approach, these represent rather extreme configurations, partially with strongly leaky fields, thus with relatively large field strengths in the regions where the CMT ansatz-field clearly violates the Maxwell equations. One expects that for ring resonators with larger diameter, with better confined bend modes, and more adiabatic interaction in the coupler regions, the CMT approach comes even closer to reality.

5.1 Remarks on the numerical procedures

The coupled mode equations (18), (19) are treated by numerical means on a rectangular computational window $[x_l, x_r] \times [z_i, z_o]$ as introduced in Figure 2. The solution involves the numerical quadrature of the integrals (16), (17) in the z -dependent matrices \mathbf{M} and \mathbf{F} , where a simple trapezoidal rule [36] is applied, using an equidistant discretization of $[x_l, x_r]$ into intervals of length h_x .

Subsequently, a standard fourth order Runge-Kutta scheme [36] serves to generate a numerical solution of the coupled mode equations over the computational domain $[z_i, z_o]$, which is split into intervals of equal length h_z . Exploiting the linearity of equation (19), the procedure is formulated directly for the transfer matrix \mathbf{T} , i.e. applied to the matrix equation

$$d_z \mathbf{T}(z) = \mathbf{M}(z)^{-1} \mathbf{F}(z) \mathbf{T}(z) \quad (25)$$

with initial condition $\mathbf{T}(z_i) = \mathbf{I}$ (the identity matrix), such that $\mathbf{C}(z) = \mathbf{T}(z) \mathbf{C}(z_i)$. While the evaluation of the resonator properties via equations (23) and (8), (9) requires only the solution $\mathbf{T} = \mathbf{T}(z_o)$ at the coupler output plane $z = z_o$, also the examination of the evolutions of $\mathbf{T}(z)$, or $\mathbf{S}(z)$, respectively, turns out to be instructive.

The results of the CMT approach are compared with FDTD simulations [22]. We apply an own implementation [24, 25] based on a simple second order Yee scheme [37]. Perfectly Matched Layer (PML) boundary conditions enclose the rectangular computational window, where fields are excited using the total-field / scattered field formulation. In order to generate reference signals for purposes of normalization, all FDTD calculations are carried out twice, once for the entire microresonator structure, then for one of the constituent straight waveguides only. To evaluate the spectral throughput- and dropped power, the time evolutions of the fields at suitable cross section lines through the respective ports are Fourier transformed, then projected onto the outgoing frequency domain mode profiles associated with the port. The ratio of the absolute values of these spectral signals (calculation for the microresonator structure / reference calculation) forms an approximation for the normalized output powers.

5.2 Coupler with monomodal bent waveguide

As the first example we consider bent-straight waveguide couplers according to Figure 2, formed by straight and circularly bent cores of widths $w_s = 0.4 \mu\text{m}$ and $w_c = 0.5 \mu\text{m}$ with refractive index $n_c = n_s = 1.5$, embedded in a background with refractive index $n_b = 1$. The configurations differ with respect to the radius R of the outer bend interface, and with respect to the distance g between the cores. The interaction of waves with vacuum wavelength $\lambda = 1.05 \mu\text{m}$ is studied, $k_0 = 2\pi/\lambda$ is the associated vacuum wavenumber. Both constituent waveguides are single-mode at the target wavelength, with mode profiles that are well confined to the respective cores. Figure 3 illustrates an example for the two basis fields. The longer outer tail of the bend profile is accompanied by a slight shift of the profile maximum towards the exterior of the bend.

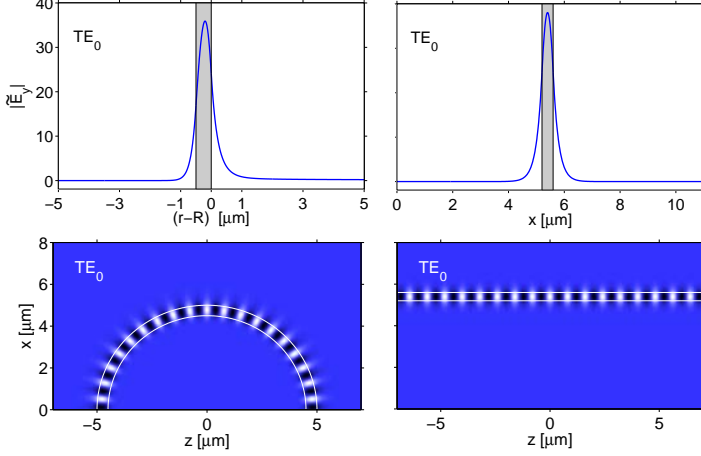


Figure 3: Normalized fundamental TE mode profiles $|\tilde{E}_y|$ (top) and snapshots of the propagating physical fields E_y (bottom) of the constituent bent (left) and straight waveguides (right) related to the coupler configurations of Section 5.2, for $R = 5 \mu\text{m}$. The effective mode indices of the basis fields are $\gamma/k_0 = 1.29297 - i7.5205 \cdot 10^{-6}$ (bend mode), and $\beta/k_0 = 1.3137$ (straight waveguide).

The CMT simulations of the couplers are carried out on computational windows of $[x_1, x_r] \times [z_1, z_o] = [0, R + 10 \mu\text{m}] \times [-R + 1 \mu\text{m}, R - 1 \mu\text{m}]$, if $R \leq 5 \mu\text{m}$, otherwise on a window $[x_1, x_r] \times [z_1, z_o] = [R - 5 \mu\text{m}, R + 10 \mu\text{m}] \times [-8, 8] \mu\text{m}$, discretized with stepsizes of $h_x = 0.005 \mu\text{m}$ and $h_z = 0.1 \mu\text{m}$. For the two basis fields the CMT analysis generates 2×2 transfer matrices \mathbf{T} and scattering matrices \mathbf{S} that can be viewed as being z -dependent in the sense as discussed in Section 5.1. Figure 4 shows the evolution of the matrix elements with the position $z = z_o$ of the coupler output plane.

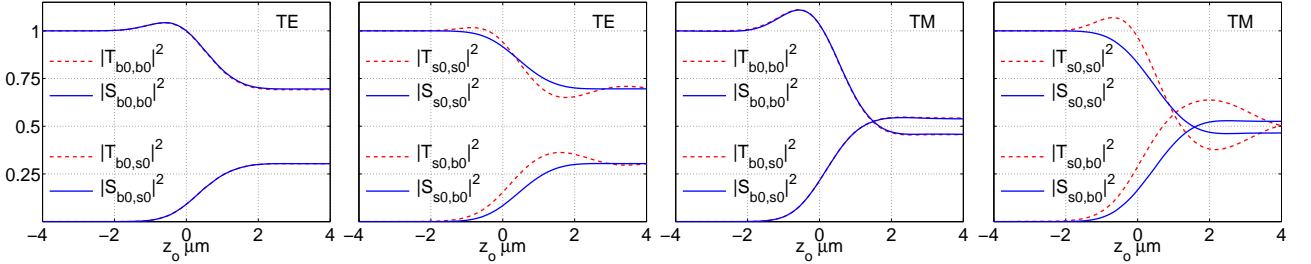


Figure 4: Elements of the transfer matrix \mathbf{T} and scattering matrix \mathbf{S} for TE (left) and TM polarized light (right), versus the output plane position z_o , for couplers as introduced in Section 5.2 with $R = 5 \mu\text{m}$ and $g = 0.2 \mu\text{m}$.

The matrix elements $T_{o,i}$ and $S_{o,i}$ relate the amplitudes of an input mode i to an output mode o ; for the present normalized modes the absolute squares can thus be viewed as the relative fractions of optical power transferred from mode i at the input plane $z = z_i$ to mode o at the output plane $z = z_o$ of the coupler. After an initial interval, where these quantities remain stationary, one observes variations around the central plane $z = 0$ of the coupler, which correspond to the interaction of the waves. Here the nonorthogonal basis fields are strongly overlapping; it is therefore not surprising that the levels of specific components of $|T_{o,i}|^2$ and $|S_{o,i}|^2$ exceed 1 in this interval.

After the region of strongest interaction, near the end of the z -computational interval, one finds that the elements $|T_{b0,i}|^2$ that map to the bend mode amplitude become stationary again, while the elements $|T_{s0,i}|^2$ related to the output to the straight mode still show an oscillatory behaviour. This is due to the interference effects as explained in the last paragraphs of Section 3. The proper amplitudes of the modes of the bus channel can be extracted by applying the projection operation (22); the corresponding matrix elements $|S_{s0,i}|^2$ attain stationary

values, such that the “coupling strength” predicted for the involved modes does not depend on the (to a certain degree arbitrary) position of the coupler output plane.

Anyway, the scattering matrix \mathbf{S} , that enters the relations (8), (9) for the transmission properties of the resonator device, should be considered a static quantity, computed for the fixed computational interval $[z_i, z_o]$. From the design point of view, one is interested in the elements of this matrix (the “coupling coefficients”) as a function of the resonator / coupler design parameters. Figure 5 summarizes the variation of \mathbf{S} with the width of the coupler gap, for a series of different bend radii.

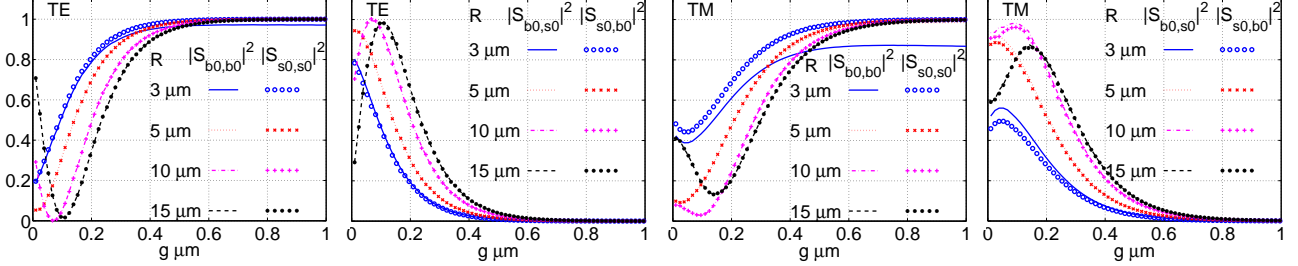


Figure 5: Scattering matrix elements $|S_{o,i}|^2$ versus the gap width g , for couplers as considered in Section 5.2 with cavity radii $R = 3, 5, 10, 15 \mu\text{m}$, for TE (left) and TM polarized waves (right).

Uniformly for all radii and for both polarizations one observes the following trends. For large gap widths, the non-interacting fields lead to curves that are constant, at levels of unity ($|S_{s0,s0}|^2$, full transmission along the straight waveguide), moderately below unity ($|S_{b0,b0}|^2$, attenuation of the isolated bend mode, stronger for the TM field), or zero ($|S_{b0,s0}|^2$ and $|S_{s0,b0}|^2$, decoupled fields). As the gap width decreases, the growing interaction strength between the modes in the two cores causes increasing cross coupling $|S_{b0,s0}|^2$, $|S_{s0,b0}|^2$ and decreasing self coupling $|S_{s0,s0}|^2$, $|S_{b0,b0}|^2$. This continues until a maximum level of power transfer is attained (where the level should depend on the “phase mismatch” between the basis fields, though a highly questionable notion in case of the bend modes [14]). If the gap is further reduced, the cross coupling coefficients decrease, even if a growing strength of the interaction can be expected; the decrease can be attributed to a process of “forth and back coupling”, where along the propagation axis a major part of the optical power changes first from the input channel to the second waveguide, then back to the input core. One should therefore distinguish clearly between the magnitude of the coefficients (17) in the differential equations that govern the coupling process, and the solution of these equations for a finite interval, the net effect of the coupler, represented by the scattering matrix \mathbf{S} .

For the symmetric computational windows used for the present simulations, the abstract reasoning of Section 2 predicts symmetric coupler scattering matrices. According to Figures 4 and 5, this constraint is respected remarkably well by the CMT simulations. In Figure 4, the curves related to $|S_{s0,b0}|^2$ and $|S_{b0,s0}|^2$ end in nearly the same level at $z = z_o$. Figure 5 shows pairs of close curves for the cross coupling coefficients, where larger deviations occur only for rather extreme configurations with small bend radii and gaps close to zero; the deviations are more pronounced for the TM case. Here one might question the validity of the assumptions underlying the CMT ansatz (12). Otherwise the symmetry of the scattering matrices provides a useful means to assess the accuracy of the CMT simulations, beyond merely the power balance constraint.

5.3 Microring resonator

For all subsequent computations of microresonator spectra, we restrict ourselves to symmetric structures ($g = \tilde{g}$) with identical monomodal straight waveguides. In line with the assumptions leading to equations (8), (9), the fundamental mode of the bus waveguides is launched at the In-port with unit power; there is no incoming field at the Add-port. Figure 6 shows the spectral response for a microring-resonator made of two couplers as considered in Section 5.2, with cavity radius $R = 5 \mu\text{m}$ and gaps $g = \tilde{g} = 0.2 \mu\text{m}$. The CMT calculations use the computational setting as introduced for Figure 4.

One observes the familiar ringresonator resonance pattern with dips in the transmitted power and peaks in the dropped intensity. According to Figure 5, the present parameter set specifies configurations with rather strong interaction in the coupler regions ($|S_{b0,s0}|^2 = 30\%$ (TE), $|S_{b0,s0}|^2 = 54\%$ (TM)), such that the resonances are

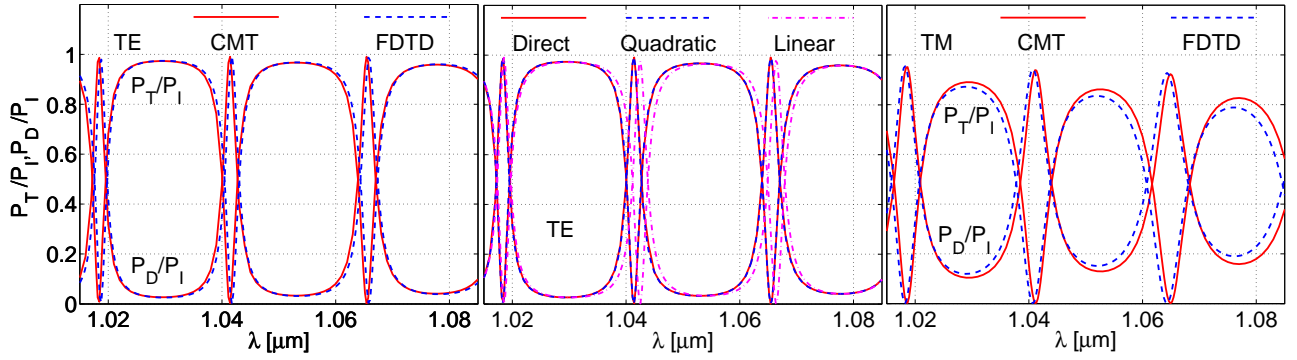


Figure 6: Relative transmitted P_T and dropped power P_D versus the vacuum wavelength for a ring resonator according to Figure 1, with parameters $n_c = n_s = 1.5$, $n_b = 1.0$, $w_c = 0.5 \mu\text{m}$, $w_s = 0.4 \mu\text{m}$, $R = 5 \mu\text{m}$, $g = \tilde{g} = 0.2 \mu\text{m}$; CMT and FDTD results for TE (left) and TM polarization (right). The central plot shows CMT results, where the spectrum has been evaluated directly and by interpolation of CMT computations for nodal wavelengths $1.015 \mu\text{m}$ and $1.085 \mu\text{m}$ (linear), or $1.015 \mu\text{m}$, $1.05 \mu\text{m}$, and $1.085 \mu\text{m}$ (quadratic interpolation).

relatively wide, with a substantial amount of optical power being directly transferred to the Drop port also in off resonant states. These properties are related to the attenuation of the cavity modes, and to the interaction strength in the coupler regions, i.e. to the radial confinement of the bend fields, hence one finds resonances of lower quality for TM polarization, and a decrease in quality with growing wavelength for both TE and TM polarized light.

The central plot of the Figure 6 shows the resonator spectrum as obtained by interpolating bend mode propagation constants and CMT scattering matrices for only two (linear interpolation) or three different wavelengths (quadratic interpolation), according to Section 4. While small deviations remain for the linear approximation, on the scale of the figure the curves related to quadratic interpolation are hardly distinguishable from the direct CMT results. Thus the interpolation approach provides a very effective means to predict the resonator spectrum, in particular if narrow dips / peaks in the responses of high-quality resonators would have to be resolved.

The CMT results are compared with FDTD simulations, where a computational window that encloses the entire resonator device has been discretized by a rectangular grid of 1200×1220 points along the x - and z -directions with uniform mesh size of $0.0125 \mu\text{m}$. The boundaries of the computational window are enclosed by $0.4 \mu\text{m}$ wide perfectly matched layers with quadratically varying strength, which provide a reflectivity of 10^{-6} for the central wavelength $\lambda = 1.05 \mu\text{m}$. The simulations are carried out over a time interval of 13.1 ps with a step size of 0.025 fs . According to the left and right plots of Figure 6, we find an excellent agreement between the CMT and the FDTD results for TE polarization, and only minor deviations for the TM case with less regular fields, more pronounced radiation, and stronger interaction in the coupler regions, where apparently the assumptions underlying the CMT approach are less well satisfied. Note that already in the present 2-D setting these FDTD calculations typically require a computation time of several hours, while the CMT analysis (with interpolation) predicts the entire spectrum in just a few minutes.

Beyond modal amplitudes and power levels, the CMT solutions permit to access the full optical electromagnetic field. Figure 7 collects plots of the principal components for off resonance and resonant configurations for both polarizations. Off resonance, one observes the large Through transmission, small amplitudes of the waves in the Drop-port, and also only minor wave amplitudes in the cavity. At the resonances, the straight transmission is almost completely suppressed; the major part of the input power arrives at the Drop-port. For the present strongly coupled configurations, the power that enters and leaves the cavity at the two couplers leads to considerably different field intensities in the left and right halves of the ring. Here the radiative parts of the bend modes are appreciable outside the cavity, in particular for the more lossy TM waves.

5.4 Multimode bent-straight waveguide coupler

If the core width of a bent waveguide is increased beyond a certain limit, a regime is reached where the modes are guided by just the outer dielectric interface, while the precise location of the interior interface becomes

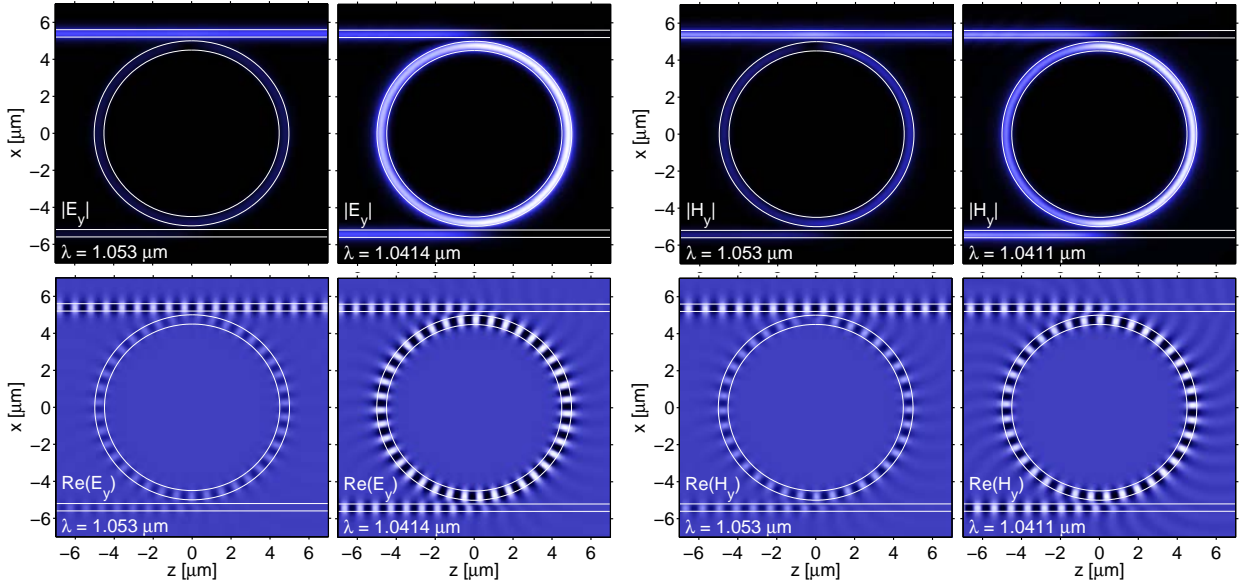


Figure 7: CMT results for the microring structure of Figure 6, local intensities (top) and snapshots of the physical field (bottom) of the principal components of TE (left) and TM polarized waves (right), for off-resonance wavelengths (first and third column) and at resonance (second and fourth column). For visualization purposes the coupler computational window has been extended to $[z_i, z_o] = [-4, 8] \mu\text{m}$.

irrelevant. Figure 8 illustrates the first four lowest order whispering gallery modes that are supported by a structure with the parameters of the previous ring segments, where the interior has been filled with the core material. If the resulting disk is employed as the cavity in a resonator structure, all bend modes with reasonably low losses must be suspected to be relevant for the functioning of the device. Therefore we now consider bent-straight coupler configurations, where the bend supports multiple whispering gallery modes.

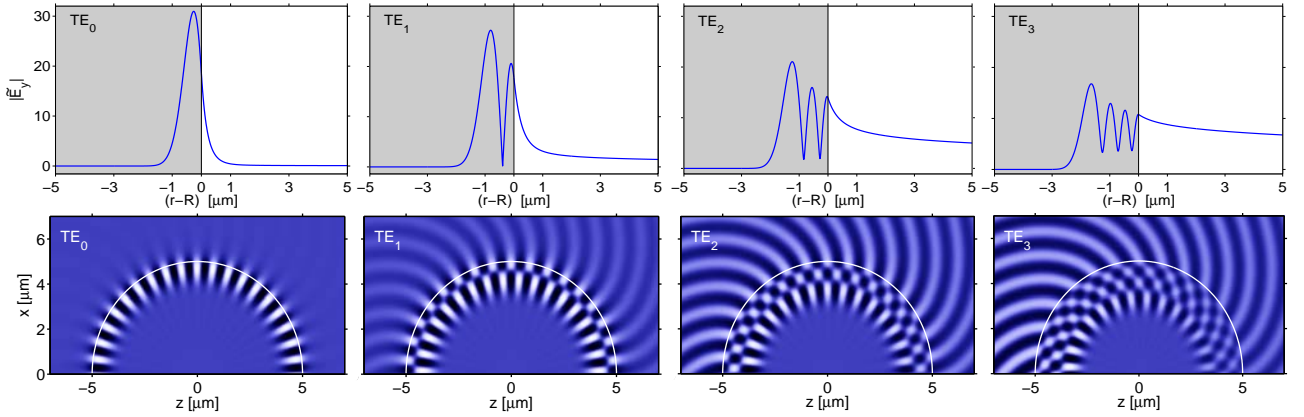


Figure 8: TE polarized whispering gallery modes; basis fields for the CMT analysis of the multimode couplers of Section 5.4. The plots show the absolute value $|\bar{E}_y|$ of the radial mode profile (top) and snapshots of the propagating physical field E_y (bottom). The effective mode indices γ_j/k_0 related to the bend radius $R = 5 \mu\text{m}$ are $1.32793 - i9.531 \cdot 10^{-7}$ (TE_0), $1.16931 - i4.032 \cdot 10^{-4}$ (TE_1), $1.04222 - i5.741 \cdot 10^{-3}$ (TE_2), and $0.92474 - i1.313 \cdot 10^{-2}$ (TE_3), for $\lambda = 1.05 \mu\text{m}$. All modes are power normalized.

A parameter set similar to Section 5.2 is adopted, with $n_c = n_s = 1.5$, $n_b = 1.0$, $R = 5 \mu\text{m}$, $w_c = R$, $w_s = 0.4 \mu\text{m}$, $g = 0.2 \mu\text{m}$, for the target wavelength $\lambda = 1.05 \mu\text{m}$. The CMT analysis of the coupler structures is carried out on a computational window $[x_1, x_r] = [0, 15] \mu\text{m}$, $[z_i, z_o] = [-4, 4] \mu\text{m}$ with large extent in the (radial) x -direction, in order to capture the radiative parts of the lossy higher order bend fields. Stepsizes for the numerical integrations are $h_x = 0.005 \mu\text{m}$, $h_z = 0.1 \mu\text{m}$, as before.

It is not a priori evident, how many basis fields are relevant for a particular simulation. Figure 9 shows the effect of the inclusion of the higher order bend modes on the evolution of the primary coefficients of the scattering matrix \mathbf{S} . The self coupling coefficient $|S_{b0,b0}|^2$ of the fundamental bend field is hardly influenced at all, and there is only a minor effect on the cross coupling coefficients $|S_{s0,b0}|^2$ and $|S_{b0,s0}|^2$. Inclusion of the first order

bend field reduces merely the self coupling coefficient $|S_{s0,s0}|^2$ of the straight mode by a substantial amount, due to the additional coupling to that basis field. Apparently, for the present structure it is sufficient to take just the two or three lowest order bend modes into account. This hints at one of the advantages of CMT approach, where one can precisely analyze the significance of the individual basis modes. We will resume this issue in Section 5.5.

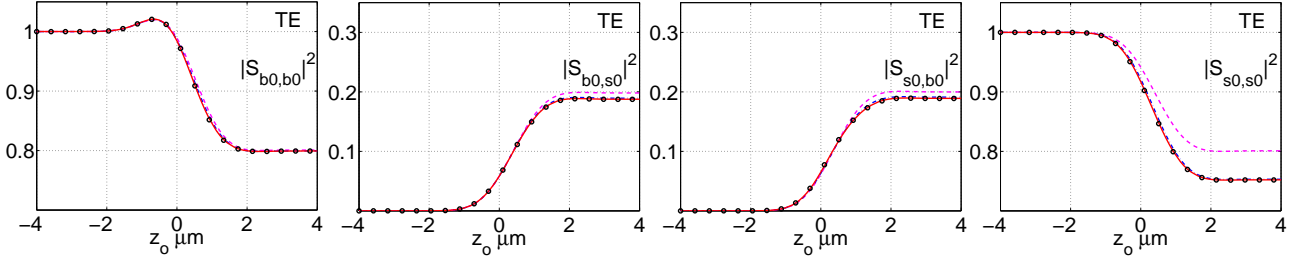


Figure 9: CMT analysis of the multimode coupler of Section 5.4, effect of the inclusion of higher order cavity modes on the evolution of the scattering matrix. Results for TE waves with one (dashed line), two (dash-dotted line), three (solid line), and four cavity modes (dotted line) taken into account. Note the different vertical axes of the plots.

With three cavity fields and the mode of the straight waveguide, the CMT simulations lead to coupler scattering matrices of dimension 4×4 . Curves for the evolution of the 16 elements of the propagation and scattering matrices \mathbf{T} , \mathbf{S} are collected in Figure 10. Just as in Section 5.2, the application of the projection procedure to extract the stationary levels $|S_{s0,j}|^2$, $|S_{j,s0}|^2$ from the nonstationary quantities $|T_{s0,j}|^2$, $|T_{j,s0}|^2$ at the exit port of the coupler is essential. Again, the agreement of the exit levels of all cross coupling coefficients indicates that reciprocity is satisfied. In contrast to Figure 4, the noticeable decay of the self coupling coefficients $|S_{b1,b1}|^2$, $|S_{b2,b2}|^2$ is due to the strong attenuation of the basis fields, as directly introduced into \mathbf{S} via equation (23).

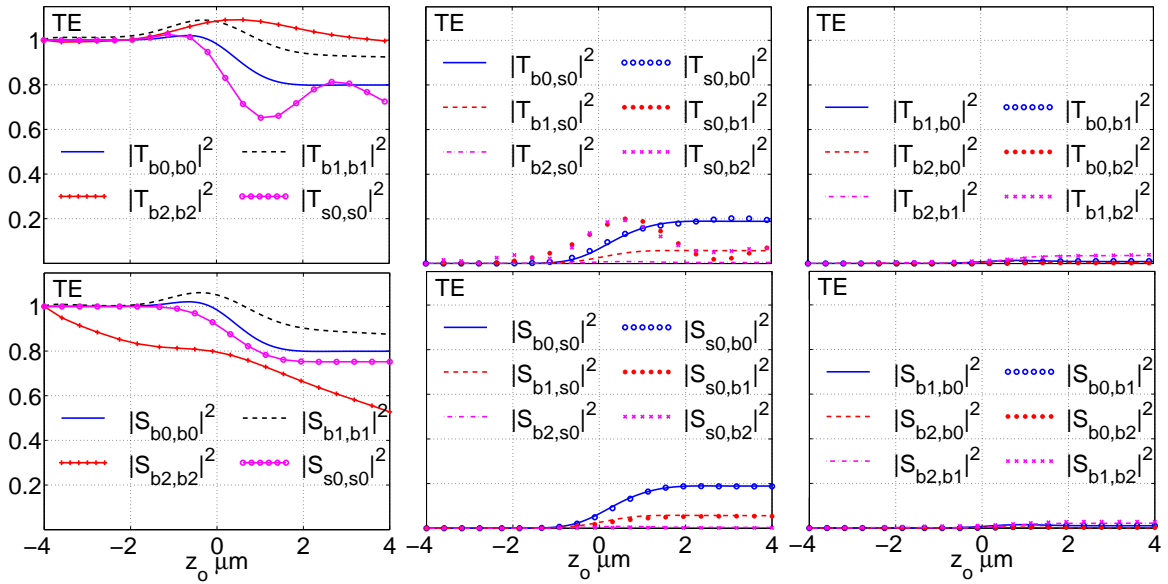


Figure 10: Evolution of the propagation matrix \mathbf{T} and scattering matrix \mathbf{S} for the coupler configuration with multimode bend as specified in Section 5.4; CMT results with four basis fields.

According to Figure 11, the elements of the scattering matrix exhibit a similar variation with the gap width as found for the former monomode bent-straight waveguide coupler (cf. Figure 5). With growing separation distance the cross coupling coefficients tend to zero. The constant levels attained by the self coupling coefficients of the bent modes are determined by the power the respective mode loses in traversing the computational window. Also here, with the exception of configurations with almost closed gap, we find that cross coupling coefficients with reversed indices coincide, i.e. that the simulations obey reciprocity.

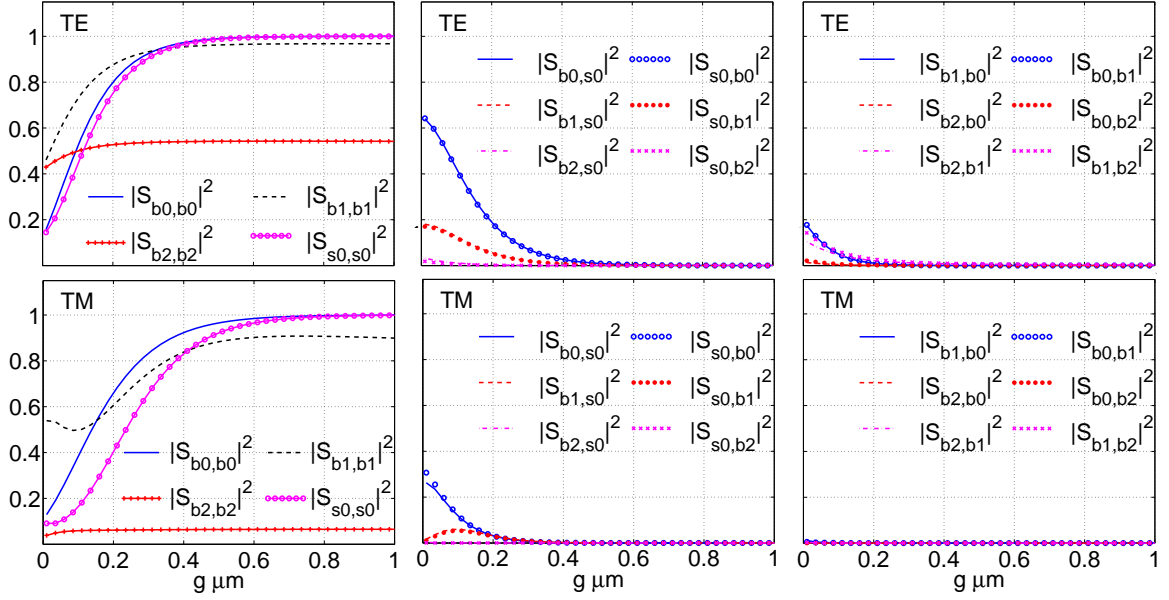


Figure 11: Scattering matrix elements $|S_{o,i}|^2$ versus the gap width g for the coupler structures of Section 5.4 for TE (top) and TM polarization (bottom). The CMT simulations take three whispering gallery modes and the fi eld of the straight waveguide into account.

5.5 Microdisk resonator

To round off the previous example, we now consider the symmetrical microdisk resonator that is constituted by two of the former multimode couplers. The computational setting and all parameters are identical to the data given in Section 5.4, for gap widths $g = \tilde{g} = 0.2 \mu\text{m}$. The CMT description represents the optical fi eld in the cavity as a superposition of the whispering gallery modes of Figure 8, where in principle one must expect that more or less pronounced features related to all of these basis fi elds appear in the resonator spectrum. Figure 12 allows to investigate the signifi cance of the individual cavity modes on the spectral response predicted by the CMT analysis.

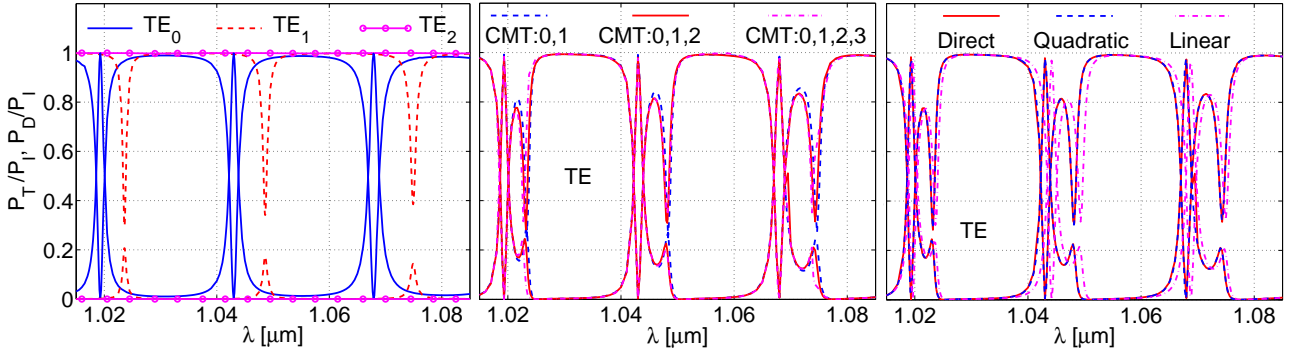


Figure 12: TE power spectrum of the microdisk resonator of Section 5.5. Left & center: CMT analysis with different sets of basis modes; besides the mode of the straight waveguide, only one bend fi eld (TE_0 , TE_1 , TE_2 , left), or the two, three, or four lowest order whispering gallery modes (center) are taken into account. Right: CMT spectra (four basis modes) computed directly, and by interpolation of data evaluated at the nodal wavelengths $1.015 \mu\text{m}$, $1.085 \mu\text{m}$ (linear) or $1.015 \mu\text{m}$, $1.05 \mu\text{m}$, $1.085 \mu\text{m}$ (quadratic interpolation).

The left and central plots of Figure 12 show the spectral response as obtained by CMT computations where, besides the mode of the straight waveguide, different sets of bend modes are used as basis fi elds. The curves related to calculations with single cavity modes (left) exhibit only specifi c extrema of the full spectrum with similar extremal levels; obviously these resonances can be assigned to the respective (TE_0 or TE_1) whispering gallery mode. As these modes circulate along the cavity with their different propagation constants, individual resonance conditions are satisfi ed in general at different wavelengths. Apparently the regime discussed at the end of Section 2 is realized here (cf. also the tiny bend mode cross coupling coeffi cients $|S_{b0,bi}|^2$ in Figure 11).

While the fundamental and first order bend mode are essential for the present resonator, inclusion of the second order whispering gallery mode into the CMT analysis leads only to minor, the third order bend field to no visible changes of the curves in the central plot of Figure 12. Thus for this microdisk configuration it is sufficient to take into account the three lowest order cavity modes as basis fields to predict reliably the spectral response. The right plot of Figure 12 allows to validate the interpolation approach of Section 4 for the spectrum evaluation; just as in Section 5.3 one finds that the quadratic interpolation of the scattering matrix coefficients and propagation constants leads to curves that are almost indistinguishable from the directly computed results.

Figure 13 compares the CMT spectra for TE and TM polarized light with rigorous FDTD calculations, where the simulation parameters are identical to those given in Section 5.3. There is a quite satisfactory agreement; as before minor deviations occur for the configurations with highly radiative, strongly interacting, and less regular fields in the TM case. The computational effort required for the CMT analysis is about two orders of magnitude lower than the effort required for the FDTD simulations.

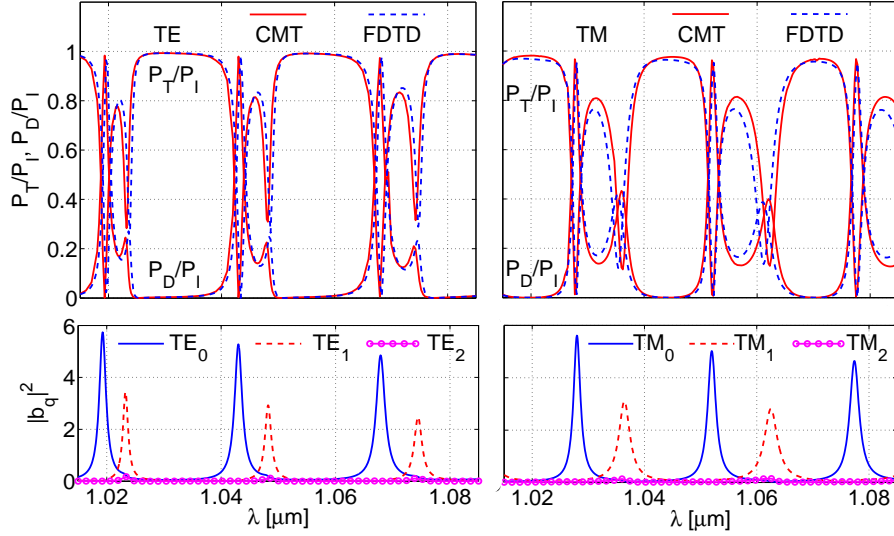


Figure 13: Power transmission through the microdisk resonator of Section 5.5, CMT and FDTD spectra (top) for TE (left) and TM polarized modes (right). The plots in the second row show the wavelength dependence of the amplitudes $|b_q|^2$ of the whispering gallery modes inside the cavity at port b (see Figure 1).

As an alternative to the computations of Figure 12, the inspection of the amplitudes of the basis modes that establish inside the cavity for varying wavelength provides a direct means for labeling the spectral features. The plots in the second row of Figure 13 identify the narrower, most pronounced resonances as belonging to the fundamental cavity modes, while the wider, less pronounced peaks are due to the first order whispering gallery fields.

Figure 14 gives an impression of the field distributions that accompany the resonance phenomena. Off resonance, most of the input power is directly transferred to the Through-port. At the wavelength corresponding to the minor resonance, the field pattern in the cavity exhibits a nearly circular nodal line that corresponds to the radial minimum in the profile of the first order whispering gallery mode (cf. Figure 8). According to Figure 13, here the first order mode carries most of the power inside the cavity. The deviation from the circular pattern is caused by the interference with the fundamental bend mode, which is also excited at this wavelength with a small power fraction. The major resonance related to the fundamental mode is of higher quality, with much larger intensity in the cavity, almost full suppression of the waves in the Through-port and nearly complete drop of the input power.

6 Conclusions

A two dimensional frequency domain model of circular integrated optical microresonators based on spatial coupled mode theory has been investigated. It turns out that only a few most relevant basis fields are required to construct approximate solutions to the scattering problems that are sufficient for purposes of practical resonator

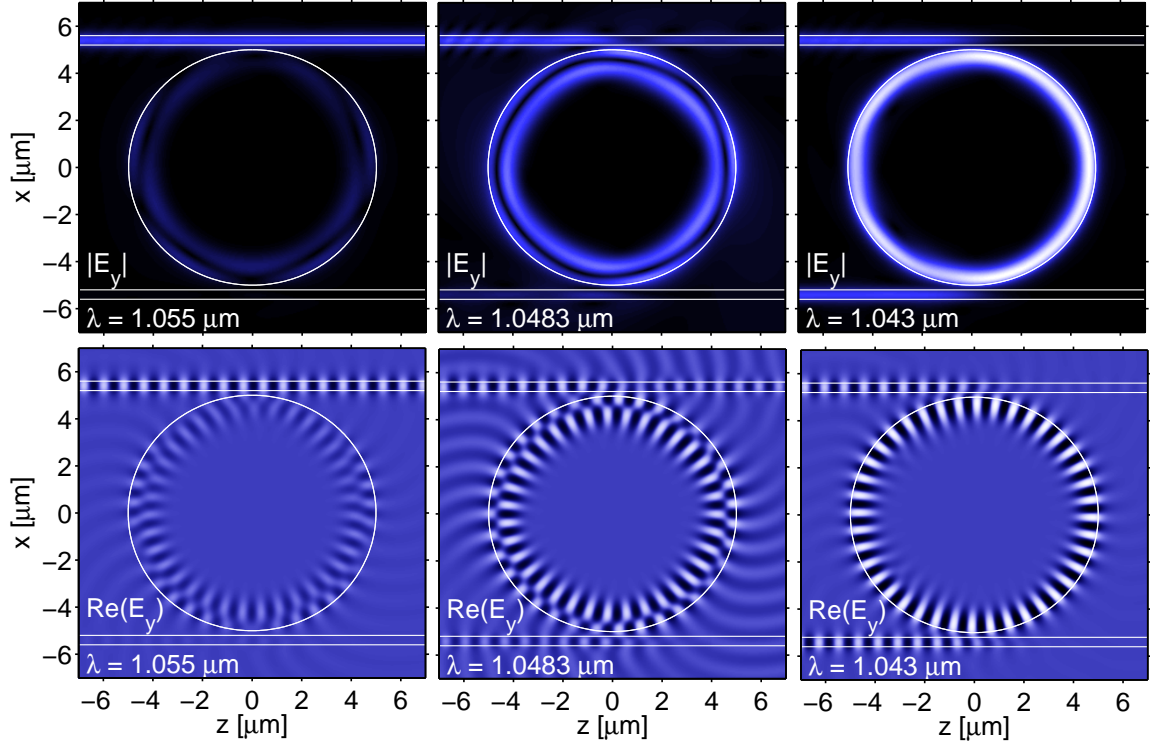


Figure 14: Field examples for the microdisk resonator of Section 5.5, CMT simulations with four basis modes, absolute value $|E_y|$ of the principal component of the TE fields (top), and snapshots of the real physical electric field (bottom). The wavelengths correspond to an off-resonance configuration (left) and to minor (center) and major resonances (right). The gray scale levels of the plots in each row are comparable.

design. The CMT results agree well with rigorous FDTD simulations; the computational effort for the CMT analysis is significantly lower. Hence the approach qualifies for a generalization to three spatial dimensions [16], where hardly any alternative, practically applicable tools are available.

The numerical examples included single- and multimode microring and -disk structures, with relatively small cavity diameters and substantial refractive index contrasts, which represent rather worst-case configurations for the CMT analysis. Beyond the optical power transmission characteristics, the CMT procedures permit the direct examination of the local amplitudes of all included basis modes, and the inspection of all components of the local optical electromagnetic field. By means of adequately interpolated bend mode propagation constants and coupler scattering matrices, the spectral properties of the resonators can be evaluated in a highly efficient way. Representing a direct implementation of the most common notions found in discussions of optical microring resonators, the present approach provides a thorough quantitative basis for the interpretation of the simulations, and thus for the resonator design.

Acknowledgment

Financial support by the European Commission (project IST-2000-28018, ‘NAIS’) is gratefully acknowledged. The authors thank E. van Groesen, H. J. W. M. Hoekstra, and the colleagues in the NAIS project for many fruitful discussions on the subject.

References

- [1] E. A. J. Marcatili. Bends in optical dielectric guides. *The Bell System Technical Journal*, September:2103–2132, 1969.
- [2] M. Bertolotti, A. Driessen, and F. Michelotti, editors. *Microresonators as building blocks for VLSI photonics*, volume 709 of AIP conference proceedings. American Institute of Physics, Melville, New York, 2004.

- [3] K. Okamoto. *Fundamentals of Optical Waveguides*. Academic Press, U.S.A, 2000.
- [4] M. Hammer, K. R. Hiremath, and R. Stoffer. Analytical approaches to the description of optical microresonator devices. In M. Bertolotti, A. Driessen, and F. Michelotti, editors, *Microresonators as building blocks for VLSI photonics*, volume 709 of AIP conference proceedings, pages 48–71. American Institute of Physics, Melville, New York, 2004.
- [5] L. F. Stokes, M. Chodorow, and H. J. Shaw. All single mode fiber resonator. *Optics Letters*, 7(6):288–290, 1982.
- [6] D. J. W. Klunder, E. Krioukov, F. S. Tan, T. van der Veen, H. F. Bulthuis, G. Sengo, C. Otto, H. W. J. M. Hoekstra, and A. Driessen. Vertically and laterally waveguide-coupled cylindrical microresonators in Si_3N_4 on SiO_2 technology. *Applied Physics B*, 73:603–608, 2001.
- [7] D. J. W. Klunder, M. L. M. Balistreri, F. C. Blom, H. W. J. M. Hoekstra, A. Driessen, L. Kuipers, and N. F. van Hulst. Detailed analysis of the intracavity phenomena inside a cylindrical microresonator. *IEEE Journal of Lightwave Technology*, 20(3):519–529, 2002.
- [8] D. J. W. Klunder, F. S. Tan, T. van der Veen, H. F. Bulthuis, G. Sengo, B. Docter, H. J. W. M. Hoekstra, and A. Driessen. Experimental and numerical study of SiON microresonators with air and polymer cladding. *IEEE Journal of Lightwave Technology*, 21(4):1099–1110, 2003.
- [9] A. Yariv. Universal relations for coupling of optical power between microresonators and dielectric waveguides. *Electronics Letters*, 36(4), 2000.
- [10] D. R. Rowland and J. D. Love. Evanescent wave coupling of whispering gallery modes of a dielectric cylinder. *IEE Proceedings-J*, 140(3):177–188, 1993.
- [11] M. K. Chin and S. T. Ho. Design and modeling of waveguide coupled single mode microring resonator. *IEEE Journal of Lightwave Technology*, 16(8):1433–1446, 1998.
- [12] C. Vassallo. *Optical Waveguide Concepts*. Elsevier, Amsterdam, 1991.
- [13] D. G. Hall and B. J. Thompson, editors. *Selected Papers on Coupled-Mode Theory in Guided-Wave Optics*, volume MS 84 of *SPIE Milestone Series*. SPIE Optical Engineering Press, Bellingham, Washington USA, 1993.
- [14] K. R. Hiremath, M. Hammer, R. Stoffer, L. Prkna, and J. Čtyroký. Analytical approach to dielectric optical bent slab waveguides. *Optical and Quantum Electronics*, 37(1-3):37–61, 2005.
- [15] R. Stoffer, K. R. Hiremath, and M. Hammer. Comparison of coupled mode theory and FDTD simulations of coupling between bent and straight optical waveguides. In M. Bertolotti, A. Driessen, and F. Michelotti, editors, *Microresonators as building blocks for VLSI photonics*, volume 709 of AIP conference proceedings, pages 366–377. American Institute of Physics, Melville, New York, 2004.
- [16] R. Stoffer, K. R. Hiremath, M. Hammer, L. Prkna, and J. Čtyroký. Cylindrical integrated optical microresonators: Modeling by 3-D vectorial coupled mode theory. *Optics Communications*, 2005. (accepted).
- [17] C. Manolatou, M. J. Khan, S. Fan, P. R. Villeneuve, H. A. Haus, and J. D. Joannopoulos. Coupling of modes analysis of resonant channel add drop filters. *IEEE Journal of Quantum Electronics*, 35(9):1322–1331, 1999.
- [18] M. Hammer. Resonant coupling of dielectric optical waveguides via rectangular microcavities: The coupled guided mode perspective. *Optics Communications*, 214(1–6):155–170, 2002.
- [19] B. E. Little, S. T. Chu, H. A. Haus, J. Foresi, and J. P. Laine. Microring resonator channel dropping filters. *IEEE Journal of Lightwave Technology*, 15:998–1005, 1997.
- [20] L. Prkna, J. Čtyroký, and M. Hubálek. Ring microresonator as a photonic structure with complex eigenfrequency. *Optical and Quantum Electronics*, 36(1-3):259–269, 2004.

- [21] J. Čtyroký, L. Prkna, and M. Hubálek. Guided-wave optical microresonators: Calculation of eigenmodes. In M. Bertolotti, A. Driessen, and F. Michelotti, editors, *Microresonators as building blocks for VLSI photonics*, volume 709 of AIP conference proceedings, pages 72–90. American Institute of Physics, Melville, New York, 2004.
- [22] A. Taflove. *Computational Electrodynamics: The Finite Difference Time Domain Method*. Artech House Inc., Norwood, MA, USA, 1995.
- [23] S. C. Hagness, D. Rafi zadeh, S. T. Ho, and A. Taflove. FDTD microcavity simulations: Design and experimental realization of waveguide coupled single mode ring and whispering gallery mode disk resonator. *IEEE Journal of Lightwave Technology*, 15(11):2154–2165, 1997.
- [24] R. Stoffer, H. J. W. M. Hoekstra, R. M. de Ridder, E. van Groesen, and F. P. H. van Beckum. Numerical studies of 2D photonic crystals: Waveguides, coupling between waveguides and filters. *Optical and Quantum Electronics*, 32:947–961, 2000.
- [25] R. Stoffer. *Uni- and Omnidirectional Simulation Tools for Integrated Optics*. PhD thesis, University of Twente, Enschede, The Netherlands, May 2001.
- [26] A. I. Nosich. The method of analytical regularization in wave-scattering and eigenvalue problems: Foundations and review of solutions. *IEEE Antennas and Propagation Magazine*, 41(3):34–49, 1999.
- [27] S. V. Boriskina, T. M. Benson, P. Sewell, and A. I. Nosich. Effect of a layered environment on the complex natural frequencies of two-dimensional WGM dielectric-ring resonators. *IEEE Journal of Lightwave Technology*, 20(8):1563–1572, 2002.
- [28] S. V. Boriskina, T. M. Benson, P. Sewell, and A. I. Nosich. Highly efficient design of spectrally engineered whispering-gallery-mode microlaser resonators. *Optical and Quantum Electronics*, 35(4/5):545–559, 2003.
- [29] S. V. Boriskina and A. I. Nosich. Radiation and absorption losses of the whispering-gallery-mode dielectric resonators excited by a dielectric waveguide. *IEEE Transactions on Microwave Theory and Techniques*, 47(2):224–231, 1999.
- [30] S. V. Boriskina, T. M. Benson, P. Sewell, and A. I. Nosich. Tuning of elliptic whispering-gallery-mode microdisk waveguide filters. *IEEE Journal of Lightwave Technology*, 21(9):1987–1995, 2003.
- [31] L. Accatino, G. Bertin, and M. Mongiardo. Elliptical cavity resonators for dual-mode narrow-band filters. *IEEE Transactions on Microwave Theory and Techniques*, 45(12):2393 – 2401, 1997.
- [32] B. E. Little, J.-P. Laine, and H. A. Haus. Analytic theory of coupling from tapered fibers and half-blocks into microsphere resonators. *Journal of Lightwave Technology*, 17(4):704–715, 1999.
- [33] I. Kiyat, Aydinli A., and Dagli N. High-Q silicon-on-insulator optical rib waveguide racetrack resonators. *Optics Express*, 13(6):1900–1905, 2005.
- [34] E. C. M. Pennings. *Bends in Optical Ridge Waveguides, Modelling and Experiment*. PhD thesis, Delft University, The Netherlands, 1990.
- [35] K. R. Hiremath, R. Stoffer, and M. Hammer. Multimode circular integrated optical microresonators: Coupled mode theory modeling. In *Proceedings of 9'th Annual Symposium of IEEE/LEOS Benelux Chapter*, pages 79–82, 2004.
- [36] W. H. Press, S. A. Teukolsky, W. T. Vetterling, and B. P. Flannery. *Numerical Recipes in C, 2nd ed*. Cambridge University Press, 1992.
- [37] K. S. Yee. Numerical solution of boundary value problems involving Maxwell's equations in isotropic media. *IEEE Transactions on Antennas and Propagation*, 14(3):302–307, 1966.